Electronic Supplementary Material (ESI) for Chemical Science.

Supporting Information

Ground-state-dominated Magnetic Field Effect on the Luminescence of Stable Organic Radicals

Shun Kimura, Shojiro Kimura, Ken Kato, Yoshio Teki,* Hiroshi Nishihara,* and Tetsuro Kusamoto*

Table of Contents

Detailed experimental procedures	S3
Estimation of the exchange interactions (*J*) between a PyBTM dimer	S4
Quantum simulations of emission decays and ODMR signals	S5
Emission decays of **Dope_0.1**	S11
Excimer emission decays of **Dope_4**	S12
Excimer emission decays of **Dope_22**	S12
Temperature-dependencies of emission spectra and decays of **Dope_10**	S13
Simulated temperature dependency of monomer emissions of **Dope_10**	S15
Simulated ODMR signals of **Dope_10.**	S15
Two-exponential fittings of emission decays of **Dope_R**	S16

Detailed experimental procedures

Materials and equipments

All chemicals were reagent grade and purchased commercially. Water was purified using AUTOPURE WD500 (Yamato Scientific Co., Ltd.). Dichloromethane (CH_2Cl_2), diethyl ether (Et_2O), hexane and tetrahydrofuran (THF) used for syntheses were purified through organic solvent purifier (Nikko Hansen Co., Ltd.). PyBTM, *αH*-PyBTM, and **Dope_R** were prepared and characterized by following procedures reported in the literature.[1,2]

Luminescence measurement under magnetic field

The system for luminescence measurement under magnetic field consists of a picosecond diode laser with the emission wavelength of 375 nm (Advanced Laser Diode Systems PIL037X) as light source, a single grating spectrometer (Andor Kymera193i-B1), a multichannel CCD detector (Andor iDus DV420A-OE). Photon counting detector (MPD SPD-050-CTE) was operated with time-correlated single photon counting (TCSPC) technique. This optical measurement system is combined with a solenoid type superconducting magnet, which can generate up to 14.5 T or 16.5 T.[3] Optical fibers are used to lead a light from light sources to a sample at the center of the superconducting magnet and from the sample to the spectrometer. The system of the vicinity of a sample follows the previous report.[2]

Estimation of the exchange interactions (*J*) between a PyBTM dimer

The intramolecular exchange interactions (*J, where* $H = -2J\sum \boldsymbol{S}_1 \cdot \boldsymbol{S}_2$) of PyBTM dimers in the ground states were estimated by analyzing the magnetic-field-dependence of amplitudes (i.e., photon counts right after photoexcitation) of emission decays. The increase of the amplitude corresponds to increase of the populations of the triplet close radical pair (close RP) shown in Figure 3d, ^{3}(R--R)*, by magnetic field. Because the populations of ^{3}(R--R)* were determined by the populations of the triplet PyBTM dimer in the ground states, the magnetic-field-dependence of the amplitudes ($I(B)$) in this system is given by

$$I(B) = A\left(1 - \frac{\exp(-J/k_BT)}{\exp(-J/k_BT)+\exp(J/k_BT)+\exp((J+g\mu_BB)/k_BT)+\exp((J-g\mu_BB)/k_BT)} + I_{RP}\right) \quad \text{(S1)}$$

where A is proportionality factor; g is g value of PyBTM (= 2.003); μ_B is Bohr magneton; B is magnetic field strength; k_B is Boltzmann constant; I_{RP} is a constant derived from emission of RPs in Figure 3c (because both singlet and triplet RPs depicted in Figure 3c are emissive and the sum of populations of singlet and triplet RPs right after photoexcitation is independent of magnetic field, amplitudes contributed by RPs are constant.). Figure S1 shows magnetic field dependence of the amplitudes of **Dope_10** and the fit based on equation S1, determining J/k_B as –4.8 K.

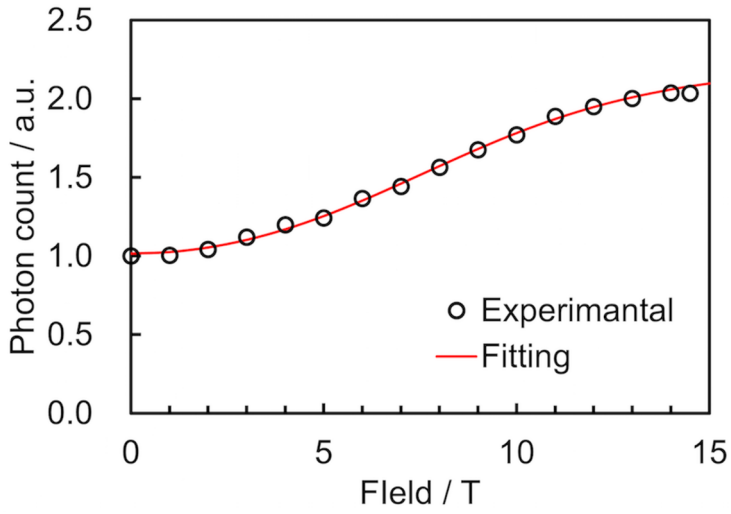

Figure S1. Magnetic-field-dependence of amplitudes of emission decays of **Dope_10** and the fit using equation S1.

Quantum simulations of emission decays and ODMR signals

The kinetic models for emission decays are shown in Figure 3cd. The scheme of Figure 3c is generalized by a scheme shown in Figure S2. In this Figure, the microwave irradiation used for the ODMR measurement is also depicted. The excited RP is generated by direct pulsed LASER excitation of the ground-state dimer R-R [k_1 process].

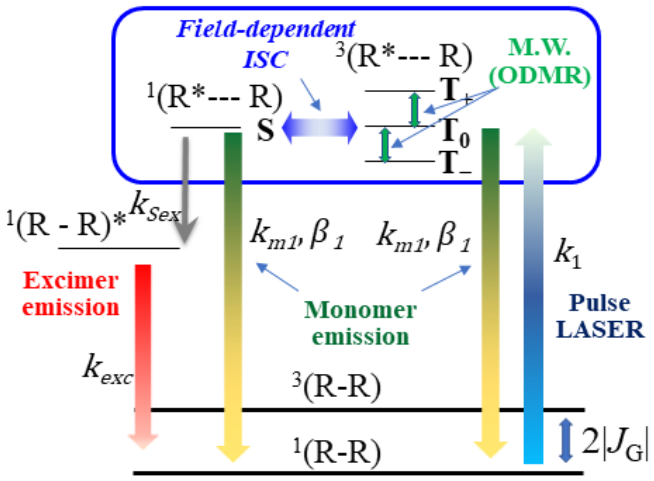

Figure S2. Kinetic models used in the quantum mechanical simulation for the emission decays and the ODMR simulations. The microwave irradiation used for the ODMR measurement is also depicted in addition to Fig. 3c.

The rate equation of the density matrix for the mechanism shown in Figure S2 is given by

$$\frac{\mathrm{d}\boldsymbol{\rho}_{R^*R}(t)}{\mathrm{d}t} = -\frac{k_{m1}}{2}\left(\boldsymbol{\rho}_{R^*R}(t)\boldsymbol{\Lambda}_S + \boldsymbol{\Lambda}_S\boldsymbol{\rho}_{R^*R}(t)\right) - \frac{k_{m1}}{2}\left(\boldsymbol{\rho}_{R^*R}(t)\boldsymbol{\Lambda}_T + \boldsymbol{\Lambda}_T\boldsymbol{\rho}_{R^*R}(t)\right)$$
$$- \frac{i}{\hbar}\left[\boldsymbol{H}_{R^*R} + \boldsymbol{H}^{\boldsymbol{MW}}_{R^*R}, \boldsymbol{\rho}_{R^*R}(t)\right] - \frac{k_{Sex}}{2}\left(\boldsymbol{\rho}_{R^*R}(t)\boldsymbol{\Lambda}_S + \boldsymbol{\Lambda}_S\boldsymbol{\rho}_{R^*R}(t)\right)$$
$$+ (Spin\ Relaxation\ Effects), \qquad \text{(S2)}$$

where

$$\boldsymbol{H}_{R^*R} = \mu_B\boldsymbol{B}\cdot\boldsymbol{g}_{\boldsymbol{R^*}}\cdot\boldsymbol{S}_{R^*} + \mu_B\boldsymbol{B}\cdot\boldsymbol{g}_{\boldsymbol{R}}\cdot\boldsymbol{S}_R + \boldsymbol{S}^{\boldsymbol{T}}\cdot\boldsymbol{D}\cdot\boldsymbol{S}^{\boldsymbol{T}} - 2J_{R^*R}\boldsymbol{S}_{R^*}\cdot\boldsymbol{S}_R\,, \qquad \text{(S3)}$$
$$\boldsymbol{H}^{\boldsymbol{MW}}_{R^*R} = 2\mu_B\boldsymbol{B}_1\cdot\boldsymbol{g}_{\boldsymbol{R^*}}\cdot\boldsymbol{S}_{R^*}\cos(\omega t) + 2\mu_B\boldsymbol{B}_1\cdot\boldsymbol{g}_{\boldsymbol{R}}\cdot\boldsymbol{S}_R\cos(\omega t)\,, \qquad \text{(S4)}$$
$$\boldsymbol{\Lambda}_S = |S><S|\quad, \qquad \text{(S5)}$$

and

$$\boldsymbol{\Lambda}_T = \textstyle\sum_i |T_i><T_i| \quad (i = +1, 0, -1 \text{ in the } M\text{s eigenfunction basis of } \boldsymbol{S}^2 \text{ operator}). \qquad \text{(S6)}$$

Here, $\mu_B\boldsymbol{B}\cdot\boldsymbol{g}_{\mathrm{p}}\cdot\boldsymbol{S}_{\mathrm{p}}$ ($\mathrm{p} = \boldsymbol{R}*\boldsymbol{or}\,\boldsymbol{R}$) are the Zeeman interaction of the species "p" with the external magnetic field ($\boldsymbol{B}$). $\boldsymbol{S}^{\boldsymbol{T}}\cdot\boldsymbol{D}\cdot\boldsymbol{S}^{\boldsymbol{T}}$ and $-2J_{R^*R}\boldsymbol{S}_{R^*}\cdot\boldsymbol{S}_R$ are the fine-structure term of the spin-triplet excited radical pair ^{3}(R*---R) and the spin exchange interaction between R* and R, respectively. These equations are similar to those of our previous work and therefore, the details should be referred to our previous work.[4] In our

previous work, the continuous light excitation was treated but in the present case the excitation is carried out by a pulsed LASER. Neglecting the LASER pulse width, we have approximated the photoexcitation occurs at $t = 0$. The excitation condition was included as the initial condition of the density matrix. It should be noted that the density matrix and the Hamiltonians depend on $\theta, \phi, \varphi, B,$ and B_1. Here, $\theta, \phi,$ and φ are the Eularian angles depicting the rotation of the $\boldsymbol{g}$ tensor and the fine-structure tensor, $\boldsymbol{D}$, from the molecular frame (X, Y, Z) to the laboratory frame (x, y, z) denoted by the external magnetic field (// z axis) and the microwave field (// x axis). B and B_1 are the magnetic flux densities of the external static magnetic field and microwave, respectively. In equations (S2) – (S4) and (S7) – (S20) shown later, we have abbreviated them as $\boldsymbol{\rho}(\theta, \phi, \varphi, B, B_1, t) \rightarrow \boldsymbol{\rho}(t)$, $\boldsymbol{H}_{R^*R}(\theta, \phi, \varphi, B, B_1, t) \rightarrow \boldsymbol{H}_{R^*R}$, $\boldsymbol{H}_{R^*R}^{\boldsymbol{MW}}(\theta, \phi, \varphi, B, B_1, t) \rightarrow \boldsymbol{H}_{R^*R}^{\boldsymbol{MW}}$, and so forth.

In the simulation of the emission decays, the microwave term, $\boldsymbol{H}_{R^*R}^{\boldsymbol{MW}}$, was eliminated in equation (S2). The rate equation of (S2) was rewritten in the Liouville space as follows.

$$\frac{\mathrm{d}\boldsymbol{\rho}_{R^*R}^{L}(t)}{\mathrm{d}t} = -\boldsymbol{L}_{R^*R}\boldsymbol{\rho}_{R^*R}^{L}(t) + \boldsymbol{\Gamma}_{R^*R}\boldsymbol{\rho}_{R^*R}^{L}(t), \qquad \text{(S7)}$$

where

$$\boldsymbol{\rho}_{R^*R}^{L}(t) = \begin{pmatrix} \rho_{R^*R}(t)_{1,1} \\ \rho_{R^*R}(t)_{1,2} \\ \vdots \end{pmatrix}, \qquad \text{(S8)} \ ,$$

and

$$\boldsymbol{L}_{R^*R} = \frac{k_{m1}}{2}(\boldsymbol{\Lambda_S}\otimes\boldsymbol{E} + \boldsymbol{E}\otimes\boldsymbol{\Lambda_S^*}) + \frac{k_{m1}}{2}(\boldsymbol{\Lambda_T}\otimes\boldsymbol{E} + \boldsymbol{E}\otimes\boldsymbol{\Lambda_T^*}) + \frac{i}{\hbar}(\boldsymbol{H}_{R^*R}\otimes\boldsymbol{E} - \boldsymbol{E}\otimes\boldsymbol{H}_{R^*R}{}^*)$$

$$+ \frac{k_{Sex}}{2}(\boldsymbol{\Lambda_S}\otimes\boldsymbol{E} + \boldsymbol{E}\otimes\boldsymbol{\Lambda_S^*}) \qquad \text{(S9)}$$

Here, $\boldsymbol{\Gamma}_{R^*R}$ is the spin-relaxation matrix of the excited radical pair and $\boldsymbol{E}$ is the unit matrix.

When the Hamiltonian and the corresponding Liouville operator are time independent, the time-evolution of $\boldsymbol{\rho}_{R^*R}^{L}(t)$ can be given by

$$\boldsymbol{\rho}_{R^*R}^{L}(t) = exp\{-(\boldsymbol{L}_{R^*R} - \boldsymbol{\Gamma}_{R^*R})t\}\boldsymbol{\rho}_{R^*R}^{L}(0)\,. \qquad \text{(S10)}$$

In order to equation (S10) to be applicable to the stretch exponential approximation, the time intervals were divided to small intervals, Δt, and

$$\boldsymbol{\rho}_{R^*R}^{L}(t) = \left[\prod_{n}^{N} exp\{-(\boldsymbol{L}_{R^*R}(t_n) - \boldsymbol{\Gamma}_{R^*R})\Delta t\}\right]\boldsymbol{\rho}_{R^*R}^{L}(0)\,. \qquad \text{(S11)}$$

Here, $t_n = n\Delta t$ and $\boldsymbol{L}_{R^*R}(t_n)$ is the stretched Liouville operator, in which k_{m1} is replaced to the following stretched rate constant, $k(t_n)$. Thus, stretch factors (β) were taken into account by employing the time-dependent transition rate (k(t)) given by

$$k(t_n) = \beta k_m(k_m t_n)^{\beta-1} \qquad \text{(S12)}.$$

where k_m is the transition rate in the case of $\beta = 1$ (uniform system).[5] To avoid infinite transition rate at $t = 0$, we used the transition rate $k(0) = \beta k_m(k_m\Delta t/2)^{\beta-1}$. The initial density matrix in the Liouville space is given by

$$\boldsymbol{\rho}_{R^*R}^{L}(0) = k_1\boldsymbol{\rho}_{RR}^{L}(\infty) \qquad \text{(S13)}.$$

Here, $\boldsymbol{\rho}^{L}_{RR}(\infty)$ is the Liouville space representation of the thermal equilibrium density matrix of the ground-state dimer R-R. The density matrix of the RP at time *t*, $\boldsymbol{\rho}_{R^*R}(t)$, is straightforwardly obtained from $\boldsymbol{\rho}^{L}_{R^*R}(t)$. It should be remembered that the density matrix and the Hamiltonians depend on $\theta, \phi, \varphi, B,$ and B_1. Hereafter, we use non-abbreviate expressions as $\boldsymbol{\rho}(t) \rightarrow \boldsymbol{\rho}(\theta, \phi, \varphi, B, t)$, and so forth. The time profile of the monomer emission is given as follows.

$$I_{\mathrm{MonEm}}(\theta, \phi, \varphi, B, t) = (1/k_1) Tr\{\boldsymbol{\Lambda}_S \boldsymbol{\rho}_{R^*R}(\theta, \phi, \varphi, B, t) + \boldsymbol{\Lambda}_T \boldsymbol{\rho}_{R^*R}(\theta, \phi, \varphi, B, t)\} \qquad \text{(S14)}$$

Since the molecules are oriented randomly in the sample, in which the external magnetic field is applied to the (θ, ϕ) direction to the principal axes (*X*, *Y*, *Z*) of the fine-structure and *g* tensors, the time profiles of the monomer emission can be calculated as follows.

$$\langle I_{\mathrm{MonEm}}(B, t) \rangle = \frac{1}{V} \int_0^{\pi} \int_0^{2\pi} \int_0^{\pi} I_{\mathrm{MonEm}}(\theta, \phi, \varphi, B, t) \sin\theta \, \mathrm{d}\theta d\phi d\varphi, \qquad \text{(S15)}$$

For the excimer emission, the density matrix of the singlet excimer state at time *t*, $\rho_{exm}(\theta, \phi, \varphi, B, t)$, was calculated by

$$\rho_{exm}(\theta, \phi, \varphi, B, t) = \int_0^{\mathrm{t}} \{k_{Sex} Tr\{\boldsymbol{\Lambda}_S \boldsymbol{\rho}_{R^*R}(\theta, \phi, \varphi, B, \tau)\} - k_{exc} \rho_{exm}(\theta, \phi, \varphi, B, \tau)\} d\tau \qquad \text{(S16)}$$

The time profile of the excimer emission is given as follows.

$$I_{\mathrm{Exc\ Em}}(\theta, \phi, \varphi, B, t) = (1/k_1) Re\{\rho_{exm}(\theta, \phi, \varphi, B, t)\} \qquad \text{(S17)}$$

and

$$\langle I_{\mathrm{Exc\ Em}}(B, t) \rangle = \frac{1}{V} \int_0^{\pi} \int_0^{2\pi} \int_0^{\pi} I_{\mathrm{Exc\ Em}}(\theta, \phi, \varphi, B, t) \sin\theta \, \mathrm{d}\theta d\phi d\varphi, \qquad \text{(S18)}$$

Emission decays of Close RP were calculated by classical mechanical simulation (conventional rate equations) based on Figure 3d and monomer emission decays of **Dope_10** were estimated as the totals of those of RP and Close RP. The monomer emission and excimer emission intensities were obtained by integrating the time-resolved emission from 0 to 696 ns and 0 to 3000 ns, respectively. “No excited-state MFE” in Figure 4c was calculated by classical mechanical simulation based on Figure 3cd with assuming that ISC between singlet (S) and triplet (T_0) RPs in the excited states does not occur. “No ground-state MFE” in Figure 4d was calculated by fixing the spin-sublevel populations of PyBTM dimer in the ground states as those at 0 T.

To calculate the optically detected ESR (ODMR), the interaction with the microwave, $\boldsymbol{H}^{\boldsymbol{MW}}_{R^*R}$, are included and we moved from the Laboratory frame to the frame rotating with the angular frequency (ω) of the microwave. In the rotating frame, the corresponding rated equations are written as follows.

$$\begin{aligned} \frac{\mathrm{d}\boldsymbol{\rho}_{R^*R}(t)_{rot}}{\mathrm{d}t} = & -\frac{k_{m1}}{2}(\boldsymbol{\rho}_{R^*R}(t)_{rot}\boldsymbol{\Lambda}_S + \boldsymbol{\Lambda}_S\boldsymbol{\rho}_{R^*R}(t)_{rot}) - \frac{k_{m1}}{2}(\boldsymbol{\rho}_{R^*R}(t)_{rot}\boldsymbol{\Lambda}_T + \boldsymbol{\Lambda}_T\boldsymbol{\rho}_{R^*R}(t)_{rot}) \\ & - \frac{i}{\hbar}\left[\boldsymbol{H}^{\boldsymbol{rot}}_{R^*R} + \boldsymbol{H}^{\boldsymbol{MW,rot}}_{R^*R}, \boldsymbol{\rho}_{R^*R}(t)_{rot}\right] - \frac{k_{Sex}}{2}(\boldsymbol{\rho}_{R^*R}(t)_{rot}\boldsymbol{\Lambda}_S + \boldsymbol{\Lambda}_S\boldsymbol{\rho}_{R^*R}(t)_{rot}) \\ & + (Spin\ Relaxation\ Effects), \qquad \text{(S19)} \end{aligned}$$

In addition, only the following secular term (***AA***) of the total Hamiltonian ($\boldsymbol{H}^{\boldsymbol{rot}}_{R^*R} + \boldsymbol{H}^{\boldsymbol{MW,rot}}_{R^*R}$) was treated.

$$\boldsymbol{AA} = (g_{zz}^{R^*}\mu_B B_0 - \hbar\omega)S_z^{R^*} + \frac{\mu_B B_1}{2}\{(g_{xx}^{R^*} - ig_{xy}^{R^*})S_+^{R^*} + (g_{xx}^{R^*} + ig_{xy}^{R^*})S_-^{R^*}\} + (g_{zz}^{R}\mu_B B_0 - \hbar\omega)S_z^{R}$$

$$+ \frac{\mu_B B_1}{2}\{(g_{xx}^{R} - ig_{xy}^{R})S_+^{R} + (g_{xx}^{R} + ig_{xy}^{R})S_-^{R}\} - D_0 S_z^2 + \frac{D_0}{4}(S_+^{R^*}S_-^{R} + S_-^{R^*}S_+^{R})$$

$$- 2J_{R^*R}\left\{S_z^{R^*}S_z^{R} + \frac{S_+^{R^*}S_-^{R} + S_-^{R^*}S_+^{R}}{2}\right\}, \qquad (S20)$$

The details are similar to those described in our previous work.[4] The meaning and definition of each terms are written in the previous work. The later simulation procedures resemble to those of the emission decays. Time-resolved ODMR profiles were obtained by taking the deference of the emission decays between the ON and OFF conditions of the microwave. The ODMR spectrum shown in Figure S12 was obtained by integrating the time-resolved ODMR from 0 to 500 ns. The parameters used in the simulations are summarized in Table S1.

Table S1 Parameters used in the simulations of emission decays and ODMR

Kinetic constants	k_{m1} = 3.24 × 10^7 s^{-1}, k_{m2} = 3.51 × 10^7 s^{-1}, $\beta_1 = \beta_2$ = 0.63, k_{Sex} = 1.71 × 10^7 s^{-1}, k_{exc} = 1.39 × 10^6 s^{-1}
Spin Hamiltonian	$g_{//}$ = 2.0057, $g_{\perp}$ = 2.0016 for R; g = 2.0030 (isotropic) for R*
Parameters	D = 0.0 cm^{-1}, E = 0.0 cm^{-1}, J_{R^*R}/k_B = 0 K for R*---R, Δt = 0.2579 ns, Ratio of (population) × (radiative transition rate) for (RP species)/ (Close RP species) = 0.7
Relaxation times	T_1 = 5 ms, T_M = 100 ns
$\boldsymbol{\rho}_{RR}(\infty)$	Thermal equilibrium values of S_0. T_+, T_0, and T_- states: $\rho_n(\infty) = \exp(E_n/k_BT)/Z$; $Z = \sum \exp(E_n/k_BT)$ Here, E_n: the energies of the groud-state dimer obtained using $g_{//}$ = 2.0057, $g_{\perp}$ = 2.0016, J_G/k_B = –4.8 K, D_G = –0.003 cm^{-1}, E_G = 0.0 cm^{-1}
Microwave conditions	Frequency: 9.1358 GHz, B_1 = 0.14 mT

The values of parameters, k_{m1}, k_{m2}, β_1, β_2, and k_{Sex} were estimated by fitting with experimental emission decays by least-square methods. We assumed that J is same in Figure 3c and 3d in the fitting for computational reduction. The estimated values of the parameters with various restriction conditions are listed in Table S2 and Figure S3 shows the simulated emission decays and intensities with these

parameters. In all cases, the contributions of “ground-state MFE” to monomer emission intensities were much superior to those of “excited-state MFE”.

Table S2 The estimated values of the parameters, k_{m1}, k_{m2}, β_1, β_2, k_{Sex}, and the ratio of (population) × (radiative transition rate) for (RP species)/(Close RP species). The values written in bold letters indicate the fixed parameters

Entry	k_{m1} / 10^7 s^{-1}	k_{m2} / 10^7 s^{-1}	β_1	β_2	k_{Sex} / 10^7 s^{-1}	Ratio of (population) × (radiative transition rate) for (RP species)/ (Close RP species)
1	3.24	3.51	0.63	**= β_1**	1.71	**0.7**
2	3.58	4.50	0.60	**= β_1**	1.51	**0.4**
3	2.97	2.99	0.66	**= β_1**	1.86	**1.0**
4	6.37	2.35	0.51	0.7425	1.45	**0.7**
5	4.78	2.44	0.68	**= β_1**	**0.50**	**0.7**
6	4.21	2.82	0.65	**= β_1**	**1.00**	**0.7**
7	2.98	3.56	0.64	**= β_1**	**2.00**	**0.7**
8	3.08	2.35	0.71	**= β_1**	**5.00**	**0.7**
9	2.30	**= 2 × k_{m1}**	0.66	**= β_1**	1.96	**0.7**

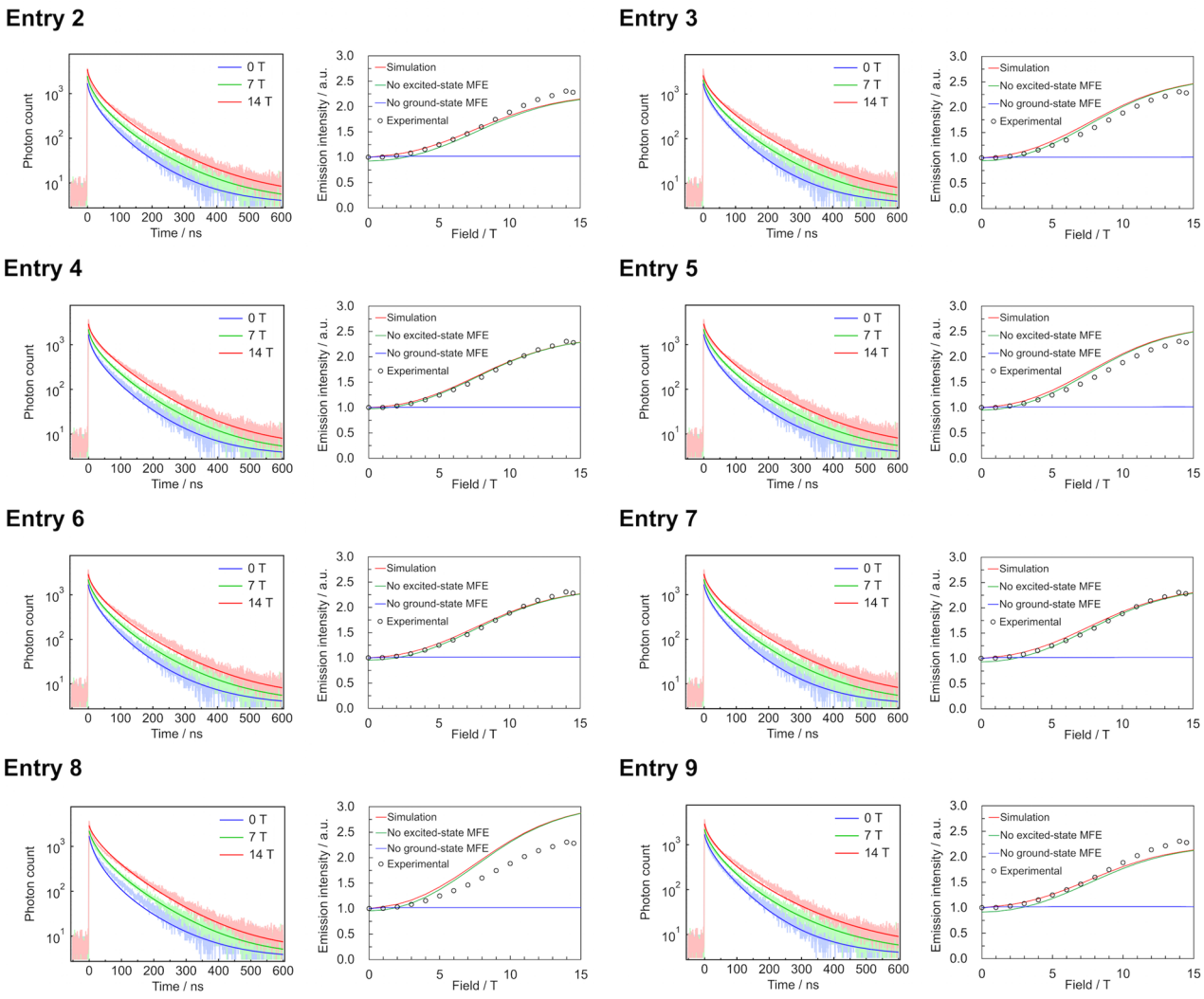

Figure S3. Simulated monomer emission decays at 0, 7, and 14 T and magnetic field dependences of monomer emission intensities for each entry listed in Table 2. The results for entry 1 are shown in main text (Figure 4a-d).

Emission decays of Dope_0.1

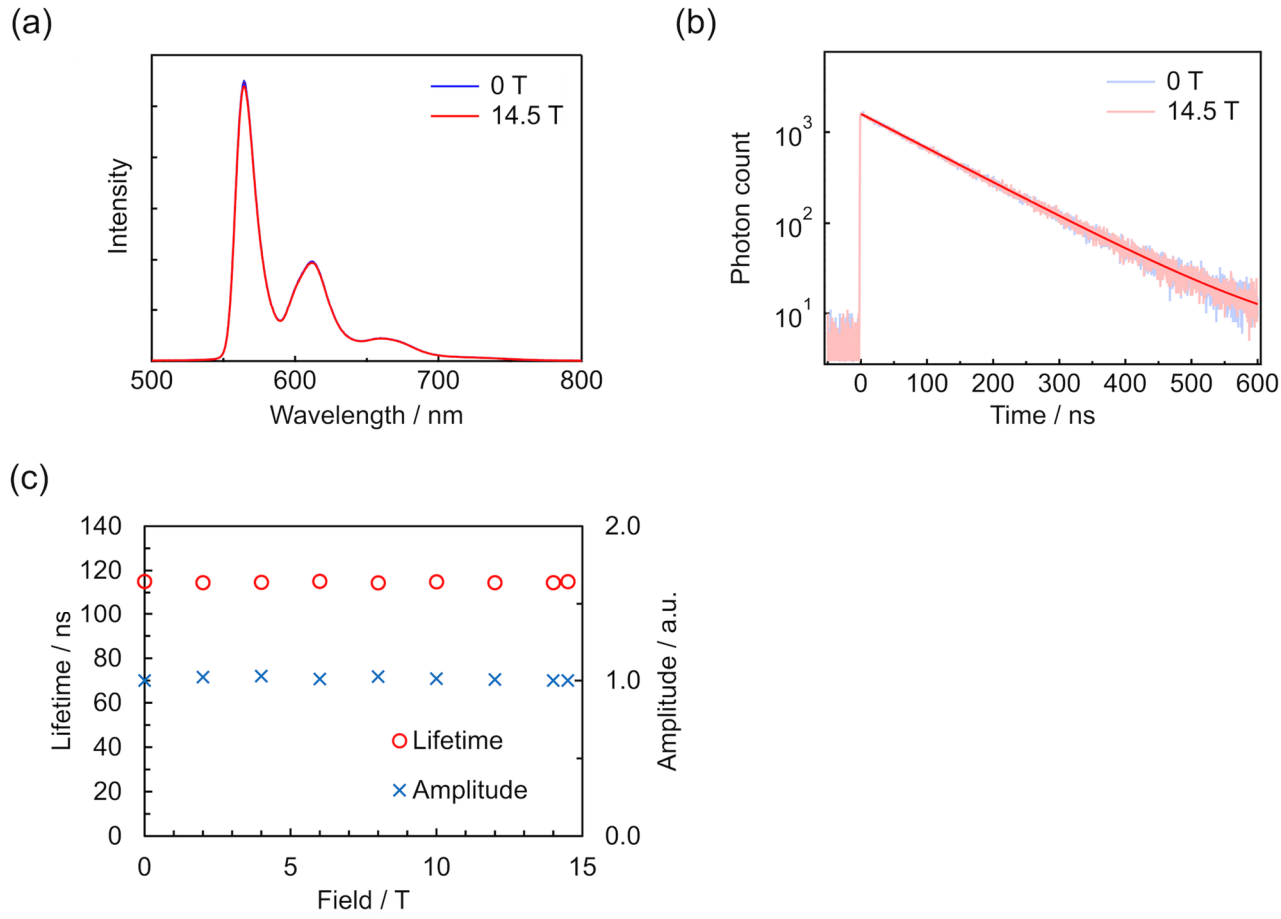

Figure S4. (a) Emission spectra of **Dope_0.1** at 4.2 K under 0 and 14.5 T, (b) their emission decays and corresponding fits at 565 nm, and (c) magnetic field dependencies of the lifetimes and amplitudes with β = 1.00.

Excimer emission decays of Dope_4

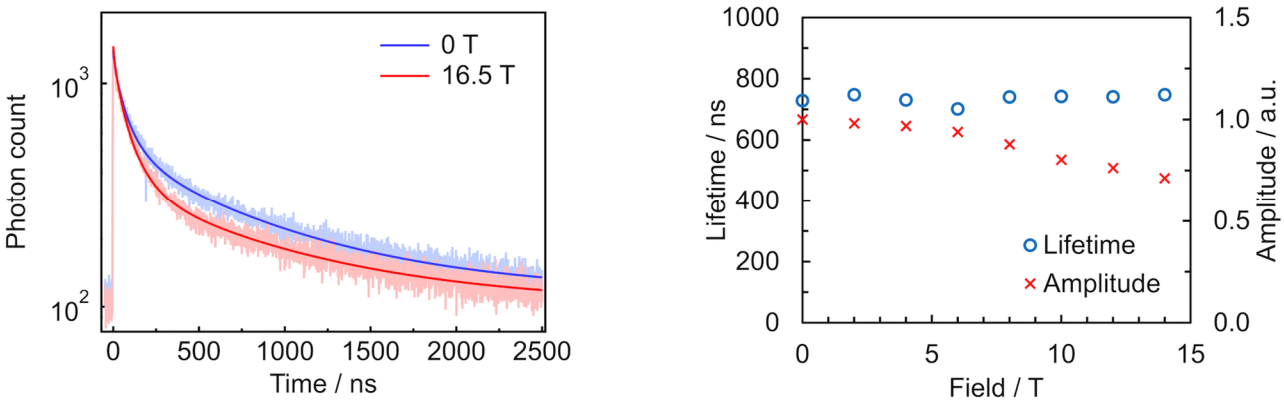

Figure S5. Emission decays and corresponding fits at 4.2 K under 0 and 16.5 T at 700 nm (left) and magnetic field dependencies of their lifetimes and amplitudes with $\beta = 0.90$ at 4.2 K (right) for **Dope_4**. Right figure only shows the component corresponding to the excimer emission.

Excimer emission decays of Dope_22

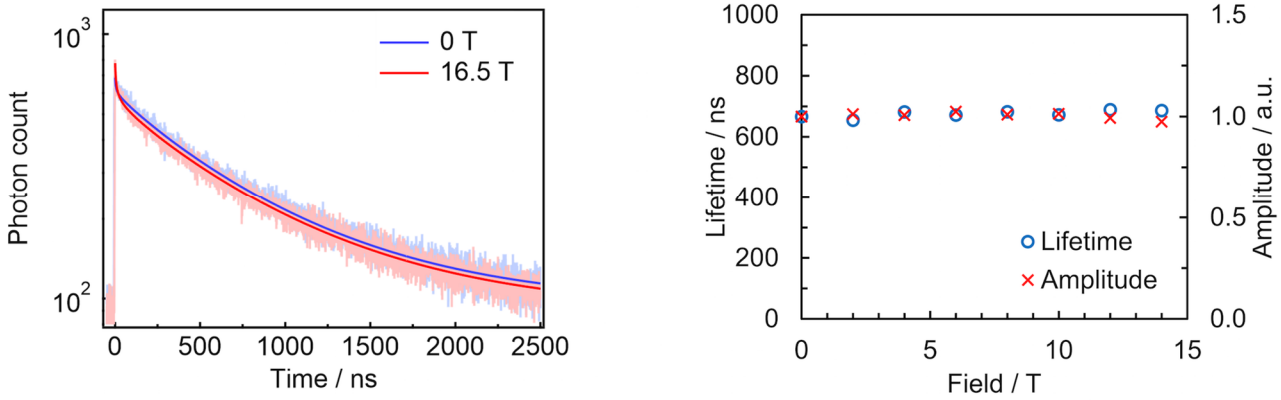

Figure S6. Emission decays and corresponding fits at 4.2 K under 0 and 16.5 T at 700 nm (left) and magnetic-field-dependencies of their lifetimes and amplitudes with $\beta = 0.90$ at 4.2 K (right) for **Dope_22**. Right figure only shows the component corresponding to the excimer emission.

Temperature-dependencies of emission spectra and decays of Dope_10

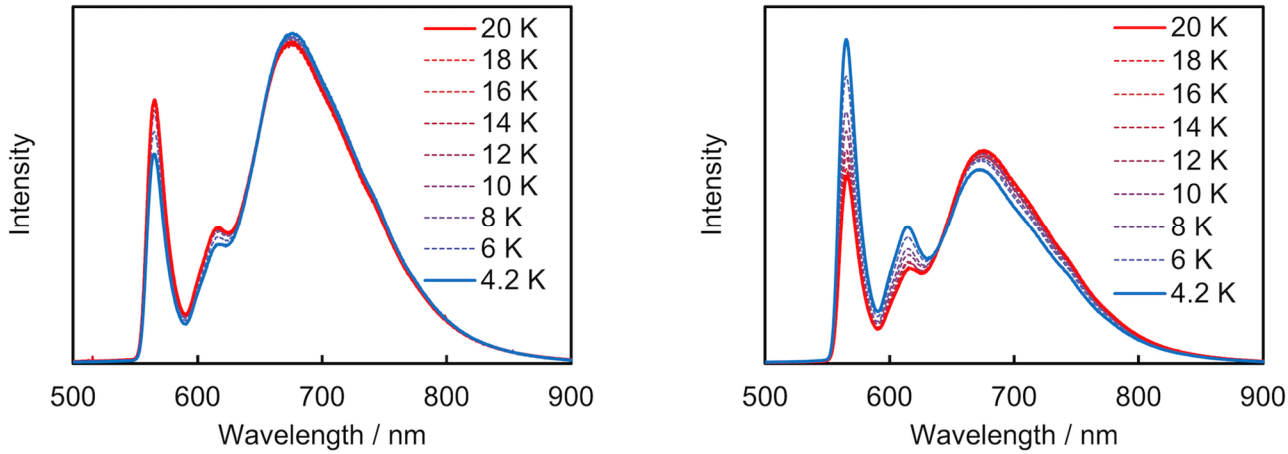

Figure S7. Emission spectra of **Dope_10** at 4.2, 6, 8, 10, 12, 14, 16, 18, 20 K under 0 T (left) and 14.5 T (right).

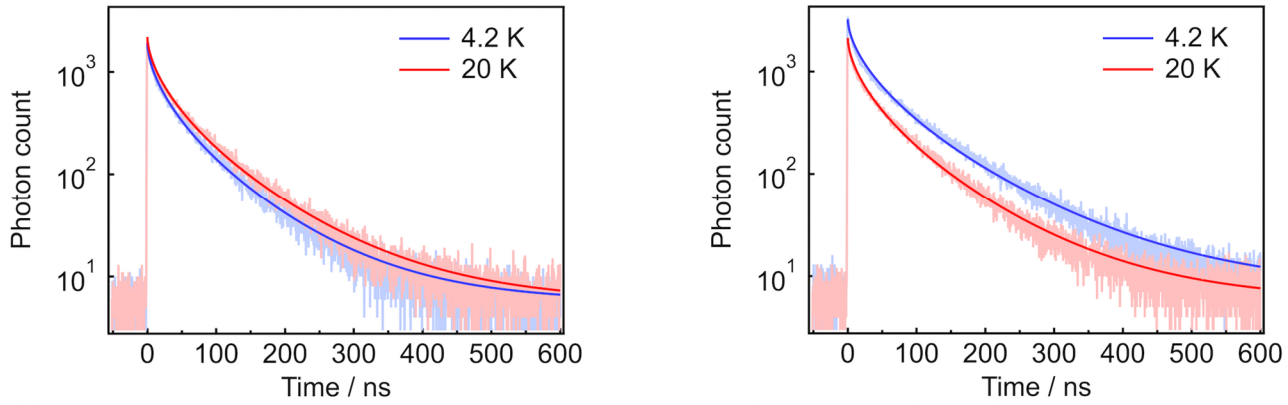

Figure S8. Emission decays and corresponding fits of **Dope_10** at 4.2 K and 20 K under 0 T (left) and 16.5 T (right) at 563 nm.

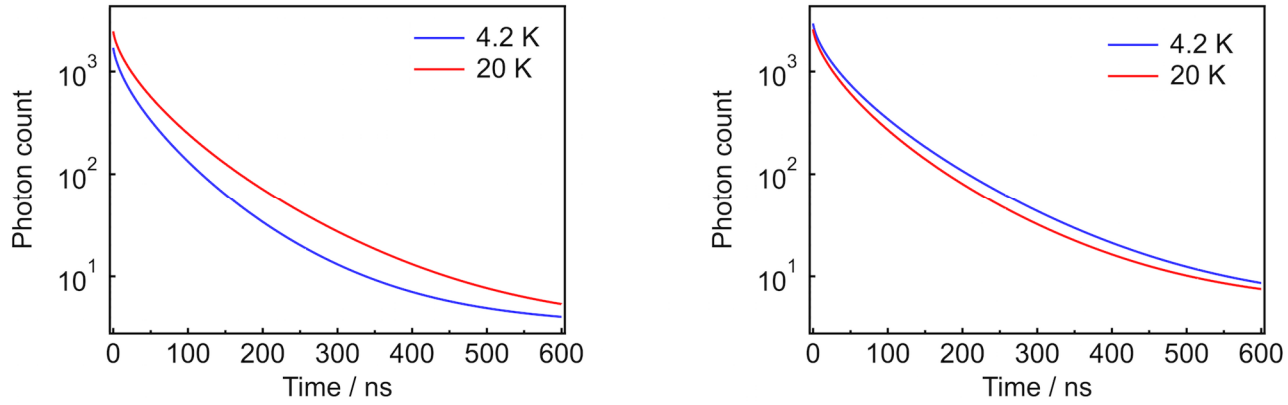

Figure S9. Simulated emission decays of **Dope_10** at 4.2 K and 20 K under 0 T (left) and 16.5 T (right) at 563 nm. The simulations were performed with the parameters of Table 1.

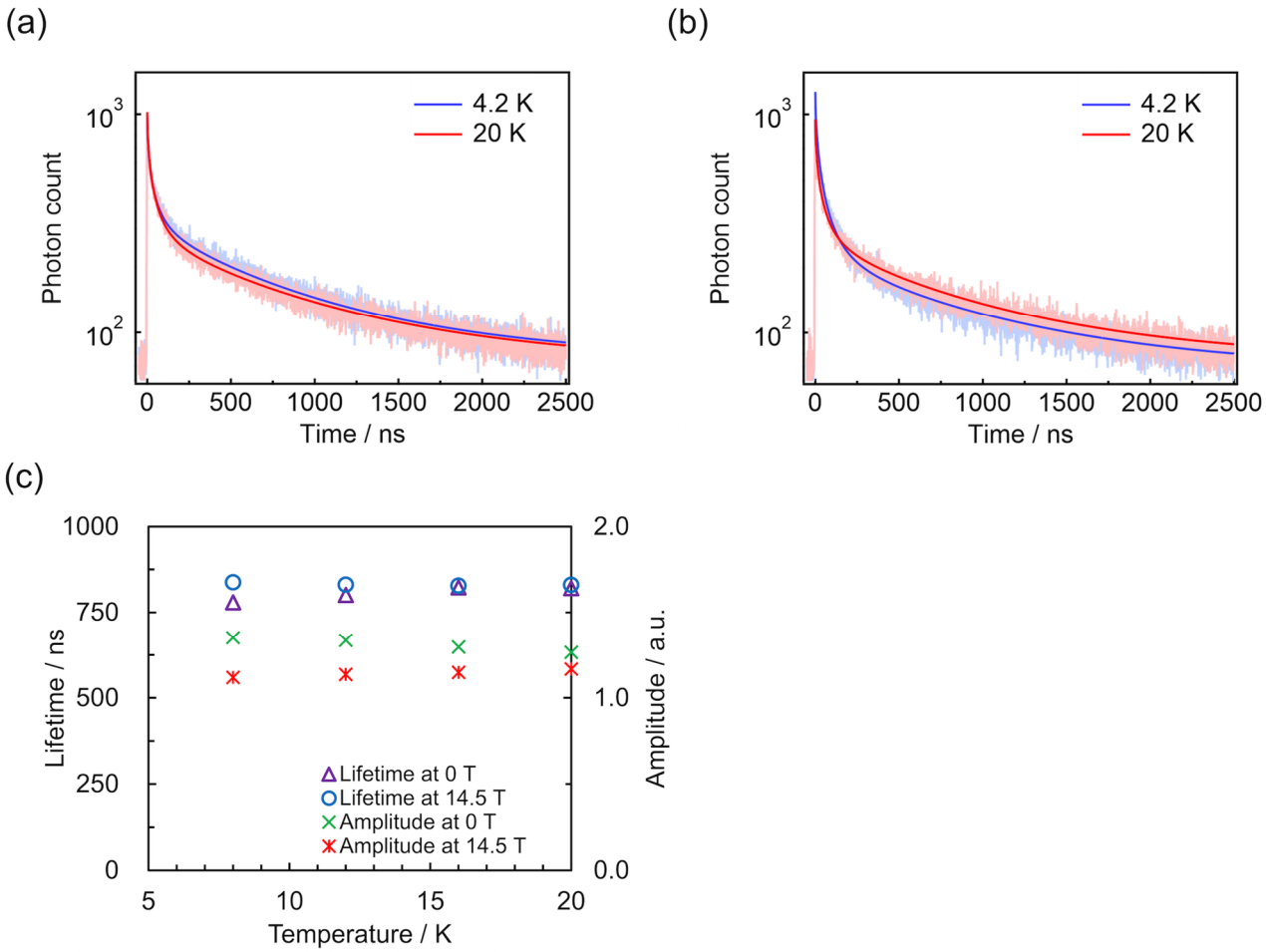

Figure S10. (a) Emission decays and corresponding fits of **Dope_10** at 4.2 K and 20 K under 0 T (left) and 14.5 T (right) at 674 nm. (b) temperature-dependencies of their lifetimes and amplitudes with $\beta = 0.88$ under 0 and 14.5 T for **Dope_10**. The figure only shows the component corresponding to the excimer emission.

Simulated magnetic-field-dependency of the excimer emission of Dope_10

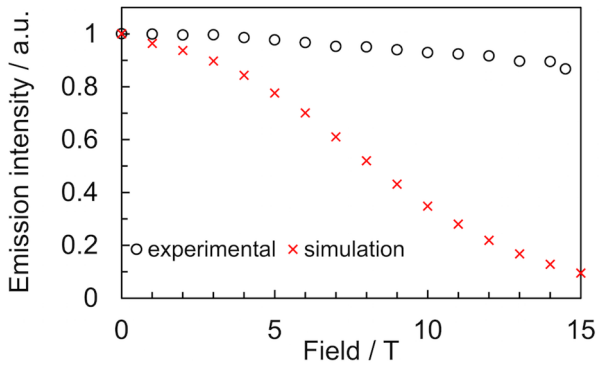

Figure S11. Simulated and experimental magnetic-field-dependencies of excimer emission intensities.

Simulated ODMR signals of Dope_10

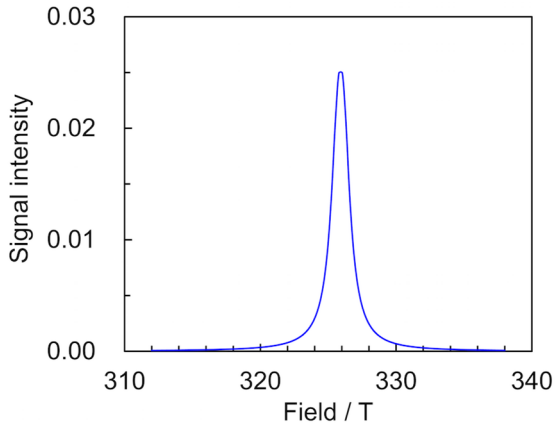

Figure S12. Simulated ODMR signal for the monomer emission of **Dope_10** at 5 K.

The ODMR signal intensity obtained experimentally in previous work[4] was higher than the simulated one, possibly because of heating by microwave resonance absorption of the ground-state species during ODMR measurements. In this case, the former can include contributions of emission enhancement of the sample by the heating. This situation is attributed to the temperature-sensitive emission based on unique characteristics of aggregated radicals: the degree of freedom in the ground-state spin multiplicities and spin-preserved photoexcitations.

Two-exponential fittings of emission decays of Dope_R

Emission decays of **Dope_R** were fitted with a sum of two exponentials, with lifetimes of τ_1 and τ_2 and corresponding amplitudes of A_1 and A_2, respectively.

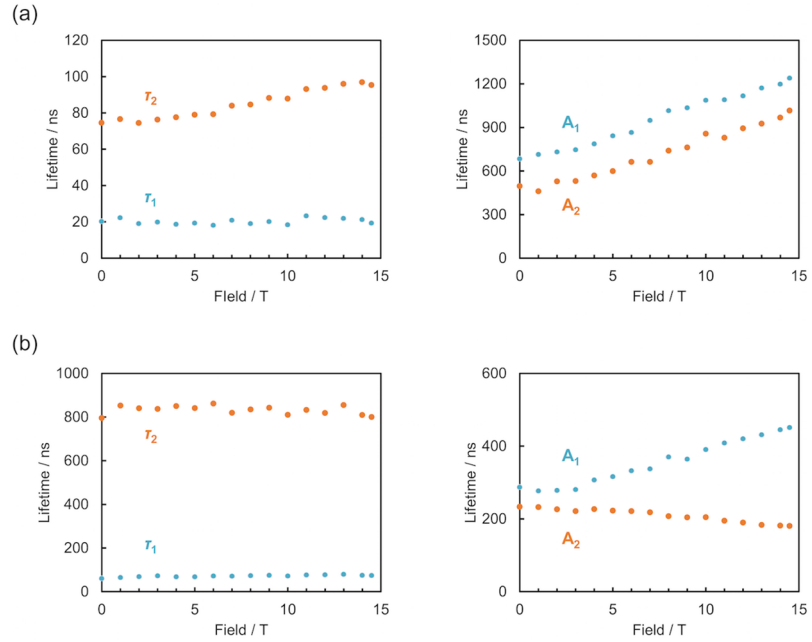

Figure S13. Magnetic field dependence of lifetimes (left) and amplitudes (right) at 4.2 K of **Dope_10** at (a) 563 nm and (b) 674 nm.

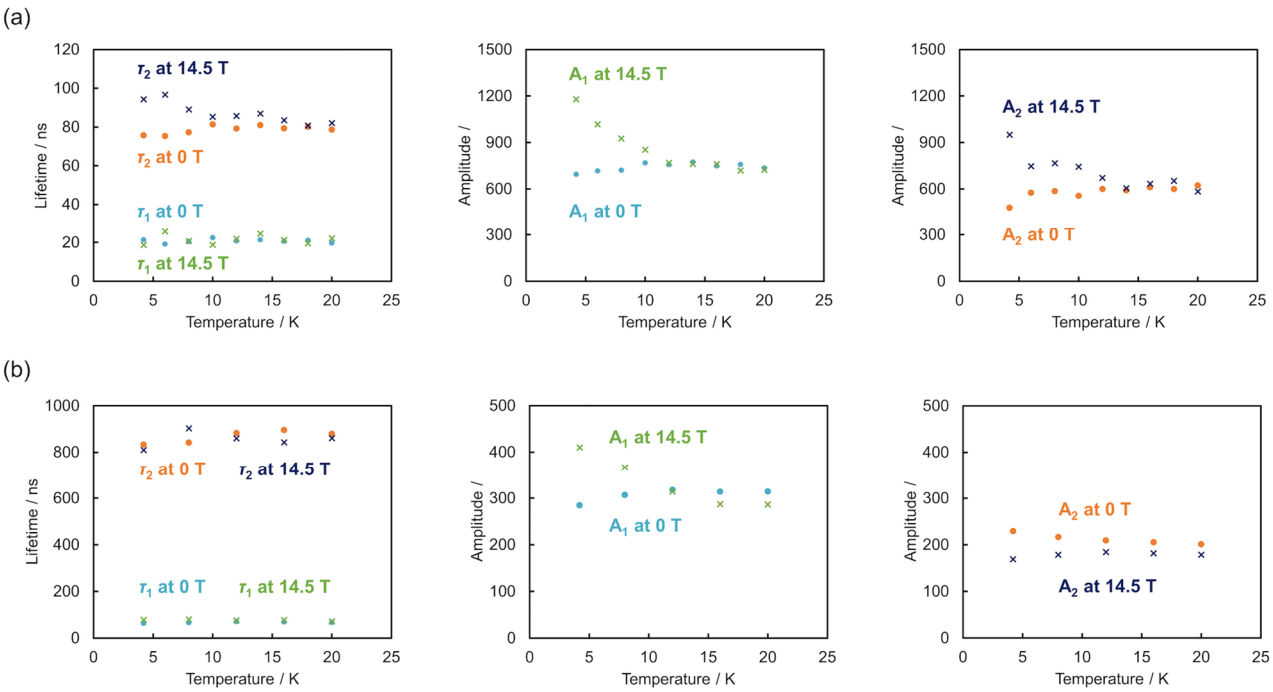

Figure S14. Temperature dependence of lifetimes (left) and amplitudes (middle and right) of **Dope_10** under 0 and 14.5 T at (a) 563 nm and (b) 674 nm.

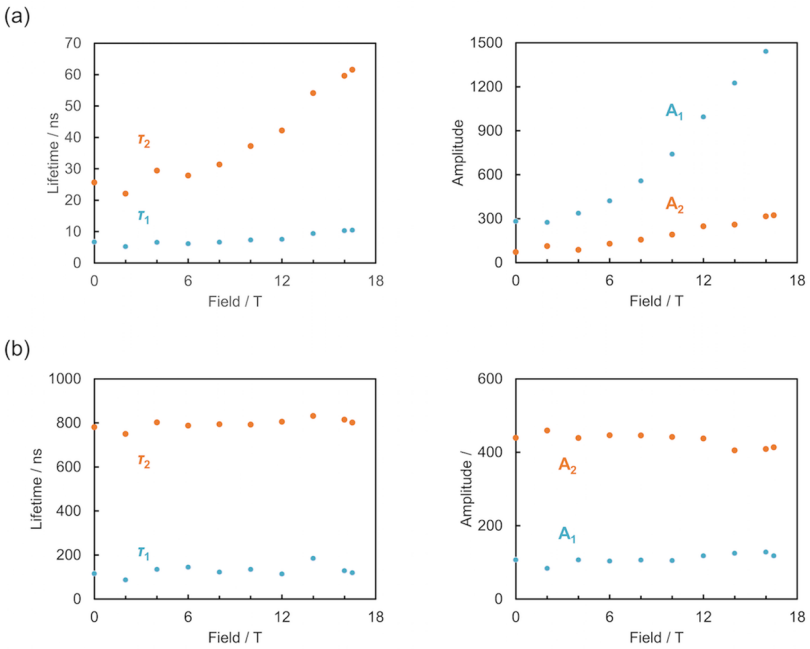

Figure S15. Magnetic field dependence of lifetimes (left) and amplitudes (right) at 4.2 K of **Dope_4** at (a) 553 nm and (b) 700 nm.

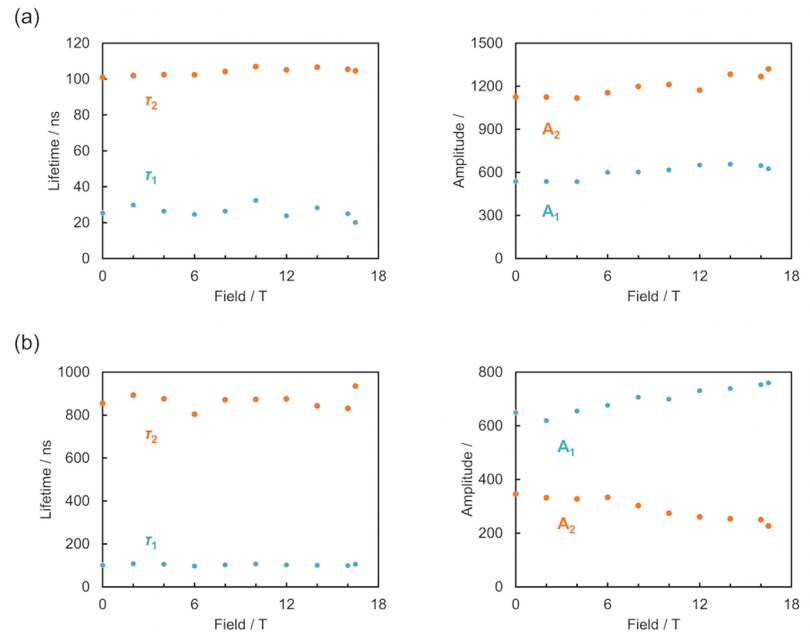

Figure S16. Magnetic field dependence of lifetimes (left) and amplitudes (right) at 4.2 K of **Dope_22** at (a) 559 nm and (b) 700 nm.

References

1 Y. Hattori, T. Kusamoto and H. Nishihara, *Angew. Chem. Int. Ed.* 2014, **53**, 11845–11848.

2 S. Kimura, T. Kusamoto, S. Kimura, K. Kato, Y. Teki and H. Nishihara, *Angew. Chem. Int. Ed.* 2018, **57**, 12711–12715.

3 Y. Sawada, S. Kimura, K. Watanabe and M. Nakano, *J. Low Temp. Phys.*, 2013, **170**, 424–429.

4 K. Kato, S. Kimura, T. Kusamoto, H. Nishihara and Y. Teki, *Angew. Chem. Int. Ed.* 2019, **58**, 2606–2611.

5 M. N. Berberan-Santos, E. N. Bodunov and B. Valeur, *Chem. Phys*. 2005, **315**, 171–182.